

Diurnal variations of aerosol optical properties in the North China Plain and their influences on the estimates of direct aerosol radiative effect

Y. Kuang¹, C. S. Zhao¹, J. C. Tao¹, N. Ma^{1, 2}

[1]{Department of Atmospheric and Oceanic Sciences, School of Physics, Peking University, Beijing, China}

[2]{Leibniz Institute for Tropospheric research, Leipzig, Germany}

*Correspondence to: C. S. Zhao (zcs@pku.edu.cn)

Abstract

In this paper, the diurnal variations of aerosol optical properties and their influences on the estimation of daily average direct aerosol radiative effect (DARE) in the North China Plain (NCP) are investigated based on in-situ measurements from Haze in China campaign. For ambient aerosol, the diurnal patterns of single scattering albedo (SSA) and asymmetry factor (g) in the NCP are both highest in the dawn and lowest in the late afternoon, and far different from those of dry state aerosol. The relative humidity (RH) is the dominant factor which determines the diurnal pattern of SSA and g for ambient aerosol. Basing on the calculated SSA and g , several cases are designed to investigate the impacts of the diurnal changes of aerosol optical properties on DARE. The results demonstrate that the diurnal changes of SSA and g in the NCP have significant influences on the estimation of DARE at the top of the atmosphere (TOA). If the full temporal coverage of aerosol optical depth (AOD), SSA and g are available, an accurate estimation of daily average DARE can be achieved by using the daily averages of AOD, SSA and g . However, due to the lack of full temporal coverage datasets of SSA and g , their daily averages are usually not available. Basing on the results of designed cases, if the RH plays a dominant role in the diurnal variations of SSA and g , we suggest that using both SSA and g averaged over early morning and late afternoon as inputs for radiative transfer model to improve the accurate estimation of DARE. If the temporal samplings of SSA or g are too few to adopt this method, either averaged over early morning or late afternoon of both SSA and g can be used to improve the

estimation of DARE at TOA.

1. Introduction

The direct effect of atmospheric aerosol on the radiation budget of earth is commonly described by direct aerosol radiative effect (DARE). DARE can be estimated from global aerosol models directly ([Myhre et al., 2013](#)), observations([Bellouin et al., 2005](#);[Bellouin et al., 2008](#)), or a combination of these two methods ([Su et al., 2013](#)). Most observation-based methods use satellite data of aerosol optical depth(AOD) in combination with aerosol optical properties retrieved from ground-based sunphotometers from Aerosol Robotic Network (AERONET) ([Holben et al., 1998](#)), where the single scattering albedo (SSA) and asymmetry factor (g) are usually held constant ([Myhre, 2009](#);[Bellouin et al., 2013](#)). However, variations of the aerosol optical properties, including AOD, SSA and g, are important information for the estimates of daily average DARE, and thus the monthly and annually averaged DARE as well.

The spatial and temporal distributions of aerosol optical properties are sampled either from space or at the earth's surface. For instance, the Moderate Resolution Imaging Spectroradiometer (MODIS) onboard Terra and Aqua pass over the equator in the morning and afternoon, respectively. Thus, temporal coverage of aerosol optical properties retrieved from satellites is limited to specific time periods. In addition, the widely used ground-based AERONET retrievals provide AOD at relatively higher temporal resolution, but the intensive optical properties (SSA and g) retrieved from AERONET measurements are typically limited to shorter time periods in the morning and afternoon when the solar zenith angle (SZA) is quite large ($50^{\circ} \leq \text{SZA} \leq 70^{\circ}$) ([Holben et al., 2006](#);[Dubovik et al., 2000](#);[Kassianov et al., 2013](#)). Although the study of ([Kaufman et al., 2000](#)) revealed that Terra and Aqua measurements can represent the annual average value within 2% error, still, the incomplete temporal samplings of aerosol optical properties may be incapable of faithfully reproducing the diurnal variation of aerosol optical properties, especially for SSA and g. Therefore, the aerosol optical properties are usually assumed to be constants ([Sena et al., 2013](#);[Myhre, 2009](#)) or with negligible variability through the day of interest ([Remer and Kaufman, 2006](#)). So far, significant diurnal changes of AOD have been frequently observed in many polluted regions around the world ([Zhang et al., 2012](#);[Mazzola et al., 2010](#);[Smirnov et al., 2002](#)), but diurnal changes of SSA and g for ambient aerosol are rarely investigated.

56 The diurnal variations of these optical properties have rarely been taken into account in the
57 measurement-based estimates of DARE. [Arola et al. \(2013\)](#) exploited data from a large number of
58 AERONET sites, and assessed the influence of diurnal AOD variability on the estimates of daily
59 average DARE at the top of atmosphere (TOA). Their results demonstrated that, for individual sites,
60 there can be significant biases in the estimates of DARE due to the diurnal AOD variability. However,
61 if averaged over all AERONET sites, the influence of diurnal changes of AOD on the daily averaged
62 DARE is rather small, the relative differences are essentially within $\pm 10\%$ and the major part being
63 centered within $\pm 5\%$, even for cases in which AOD is taken either from Terra or Aqua overpass time.
64 But the diurnal changes of SSA and g were not considered, and seasonal averages were used in this
65 research. [Kassianov et al. \(2013\)](#) also assessed the impacts of diurnal variations of aerosol optical
66 properties on the estimates of daily averaged DARE. Their results demonstrated that even in the
67 presence of strong diurnal changes of AOD, an accurate prediction of daily average DARE requires
68 only daily averaged aerosol optical properties. Nevertheless, the diurnal variations of SSA and g were
69 not also considered in this research due to their small ranges.

70 With the rapid growth of population and economy in China, emissions of anthropogenic pollutants
71 have increased dramatically in recent decades, and China is suffering very serious air pollutions. The
72 high aerosol loading in the NCP is an important factor which affects regional climate change due to
73 their potential radiative effects ([Zhao et al., 2006](#)), an accurate estimation of DARE in this region is
74 therefore important. The published results from Haze in China (HaChi) campaign demonstrated that
75 many aerosol physical and chemical properties have significant diurnal variations ([Ma et al., 2011](#); [Liu
76 et al., 2011](#); [Ran et al., 2011](#); [Xu et al., 2011](#)), which are different from the results for other regions
77 around the world. Some scientific questions regarding the diurnal variation of aerosol optical
78 properties in the NCP arose: (1) What are the characterizations of diurnal variations of aerosol optical
79 properties in the NCP, such as SSA and g ? (2) Does the diurnal variations of aerosol optical properties
80 have significant impacts on the estimation of daily average DARE in the NCP?

81 In this paper, the diurnal variations of SSA and g at ambient and dry conditions is presented at a
82 regional background site in the NCP. The calculated SSA and g are used to investigate the influences
83 of their diurnal variability on the estimates of daily average DARE at TOA and surface. This is the
84 first time, in the NCP, that the diurnal cycles of SSA and g are both taken into account in the prediction

of daily average DARE. This is particularly important for studying the direct aerosol effect in the NCP where absorbing and scattering aerosols may contribute significantly to the climate change of earth system([Chung et al., 2005](#);[Bond et al., 2013](#)).

In Sect.2, the site information and related instruments are introduced. Data and methods used in this research are described in Sect.3. Sect.4 presents the calculated diurnal variations of aerosol optical properties and their influences on the estimates of daily average DARE. Finally, conclusions are reached in Sect.5.

2. Site description and instruments

In this study, we use the dataset from the HaChi project which is conducted jointly by Peking University, China and Leibniz-Institute for Tropospheric Research, Germany at Wuqing (39°23'N, 117°01'E). This observation campaign lasted for about one month from 12 July, 2009 to 14 August, 2009. Wuqing site is located at the northern part of the NCP, between two megacities, Beijing and Tianjin. The distance between Wuqing and downtown Beijing is about 80km, and is about 30km between Wuqing and downtown Tianjin. Wuqing site is mainly surrounded by farmland and residential areas. The emission sources nearby are similar to those in most parts of the northern NCP. Hence, as a regional background site, the observational results in Wuqing can, to a large extent, represent the background aerosol properties in the northern NCP.

The particle number size distribution (PNSD) at dry state ranging from 3nm to 10 μ m was observed jointly by an Aerodynamic Particle Sizer (APS, TSI Inc., Model 3321) and a Twin Differential Mobility Particle Sizer (TDMPS, Leibniz-Institute for Tropospheric Research (IfT), Germany;[Birmili et al. \(1999\)](#)) with a temporal resolution of 10 min, and the relative humidity (RH) of sampling air is controlled lower than 30 %. The absorption coefficient at 637nm was measured using a Multi-angle Absorption Photometer (MAAP Model 5012, Thermo, Inc., Waltham, MA USA) with a temporal resolution of 1 min, and further transformed into black carbon (BC) mass concentrations with a constant mass absorption efficiency (MAE) of 6.6 m²g⁻¹. The growth factors of aerosols at RH spanning 0 to 98% are obtained from the observation of the High Humidity Tandem Differential Mobility Analyzer (HH-TDMA, Leibniz-Institute for Tropospheric Research (IfT), Germany; [Hennig et al. \(2005\)](#)). The HH-TDMA measured the growth factor at four selected particle diameters (50 nm,

100 nm, 200 nm and 250 nm) and three RH conditions (90%, 95% and 98.5%). For detailed information of the measurements, please refer to Ma et al. (2011) and Liu et al. (2011).

Furthermore, ambient RH with one-minute temporal resolution was measured by an automatic weather station (AWS). Other observational data (e.g. scattering coefficient at wavelengths of 450 nm, 550nm and 700 nm) used to retrieve the mixing state of light absorbing aerosol are in another study (Ma et al., 2012).

3. Data and methods

3.1 Calculation of aerosol optical properties

The estimation of DARE requires some aerosol optical properties, such as AOD, SSA and phase function, however, g usually used as an approximation of the phase function in the realistic calculation of DARE, although this approximation will introduce errors (Boucher, 1998). In this study, the AOD data from AERONET measurements at Xianghe site were used (Holben et al., 2006). Similar with Wuqing, Xianghe is also a background site of the NCP, the distance between them is about 40km. SSA and g were calculated using the measurements from HaChi campaign, considering both the mixing state of light absorbing carbonaceous (LAC) aerosol and the hygroscopic growth.

Ma et al. (2012) proposed a new method to retrieve the mixing state of LAC. In this method, aerosol chemical components are separated into two classes based on their refractive indices: the LAC and the less absorbing components (inorganic salts and acids, and most of the organic compounds). And dry-state aerosols are classified into two assumed types: externally mixed LAC and core-shell mixed LAC coated by less absorbing components. The mixing state of ambient aerosol is described by the mass ratio of externally mixed LAC to total LAC:

$$r_{ext-LAC} = M_{ext-LAC} / M_{LAC} \quad (1)$$

where $M_{ext-LAC}$ is the mass concentration of externally mixed LAC, and M_{LAC} is the total mass concentration of LAC measured by MAAP. According to this assumption, measured PNSD of aerosol particles is a superposition of the PNSD of externally mixed LAC and the PNSD of core-shell mixed particles:

$$N(\log D_p) = N(\log D_p)_{ext-LAC} + N(\log D_p)_{core-shell} \quad (2)$$

140 where $N(\log D_p)$ is the PNSD measured by TDMPS and APS, $N(\log D_p)_{ext-LAC}$ and
 141 $N(\log D_p)_{core-shell}$ are the PNSDs of the externally mixed LAC and the core-shell mixed particles,
 142 respectively. With the mixing state retrieved by Ma et al. (2012), $N(\log D_p)_{ext-LAC}$ can be derived
 143 using the following equation:

$$144 \quad N(\log D_p)_{ext-LAC} = N(\log D_p) \cdot r_{ext-LAC} \cdot f_{LAC} \quad (3)$$

145 where f_{LAC} is the volume fraction of LAC, which can be calculated as:

$$146 \quad f_{LAC} = \frac{M_{LAC}}{\rho_{LAC} \cdot \sum D_p (N(\log D_p) \cdot (\frac{\pi}{6} D_p^3))} \quad (4)$$

147 where ρ_{LAC} is the density of LAC, which is assumed to be 1.5 g cm^{-3} (Ma et al., 2012). Details about
 148 the method of retrieving the mixing state of LAC in the NCP can be found in Ma et al. (2012).

149 To account for the hygroscopic growth of aerosol particles, we define the growth factor as follow:

$$150 \quad g(D_{p,dry}, RH) = D_p(RH) / D_{p,dry} \quad (5)$$

151 where $D_{p,dry}$ and $D_p(RH)$ is the diameter of particle at dry state and specific RH, respectively. The
 152 externally mixed LAC is assumed to be completely hydrophobic (Bond et al., 2013) and does not grow
 153 with the increasing RH. The size-resolved hygroscopic growth factor of core-shell mixed particles are
 154 calculated using the κ -theory (Petters and Kreidenweis, 2007) to get the PNSD at ambient conditions:

$$155 \quad RH = \frac{g^3 - 1}{g^3 - (1 - \kappa)} \cdot \exp\left(\frac{4\sigma_{s/a} \cdot M_{water}}{R \cdot T \cdot D_p \cdot g \cdot \rho_w}\right) \quad (6)$$

156 where $\sigma_{s/a}$ is the surface tension of solution/air interface, its value is set to be 0.072 J m^{-2} (Petters
 157 and Kreidenweis, 2007), T is the temperature, M_{water} is the molecular weight of water, and R is the
 158 universal gas constant, ρ_w is the density of water, and κ is the hygroscopicity parameter which
 159 determines the hygroscopic ability of aerosols. By solving Eq. (6), $g(D_{p,dry}, RH)$ at different RH and
 160 D_p can be obtained, and the size-resolved κ is also required. However, up to now, no instruments are
 161 valid to provide the size-resolved κ which have covered the full aerosol particle size range. And the
 162 method used in (Chen et al., 2012) to derive the size-resolved κ is used in this research. The κ value
 163 of one aerosol particle is mainly related to its chemical composition (Liu et al., 2014), and the aerosol

particles which have similar chemical components usually come from the similar sources and experienced similar aging processes. Therefore, in this method, first, the measured PNSD at dry state are fitted with four lognormal modes, a nucleation mode with geometric mean diameters between 3 to 25 nm, an Aitken mode with geometric mean diameters between 25 to 100 nm, an accumulation with geometric mean diameters range from 100 nm to 1 μ m, and a coarse mode with geometric mean diameters range from 1 to 5 μ m. Second, the assumption is made that aerosols in a specific mode have common sources or have experienced similar aging processes, and the corresponding hygroscopic parameter κ of aerosol particles at this mode is the same due to their similar chemical compositions. Hence, the HHTDMA-measured κ of aerosol particles at diameters of 50 nm, 100 nm, 200 nm and 250 nm can be used to deduce the corresponding κ of four modes of the fitted PNSD, and then get the size-resolved κ for the full size range of PNSD. And more information about the size-resolved κ can be found in ([Chen et al., 2012](#)).

To use BHCOAT ([Bohren and Huffman, 2008](#); [Cheng et al., 2009](#)) code for the Mie calculation, we need the diameters and complex refractive indices of the core and the shell. For core-shell mixed particles, the diameter of the core does not change as the RH changes and can be calculated using the following equation:

$$D_{core} = D_{p,dry} \left(\frac{f_{LAC} - f_{LAC} \cdot r_{ext-LAC}}{1 - f_{LAC} \cdot r_{ext-LAC}} \right)^{\frac{1}{3}} \quad (7)$$

The complex refractive index of core is set to be $1.80 - 0.54i$ ([Ma et al., 2012](#)). However, the shells of aerosol particles will take up water as a function of RH and be dissolved. Both the diameters and complex refractive indices of shells will change, and the complex refractive indices of shells are calculated with the following equation:

$$\tilde{m}_{shell} = f_{solute} \cdot \tilde{m}_{solute} + (1 - f_{solute}) \cdot \tilde{m}_{water} \quad (8)$$

Where the volume fraction of solute, f_{solute} follows:

$$f_{solute} = \frac{D_{p,dry}^3 - D_{core}^3}{D_p^3(RH) - D_{core}^3} \quad (9)$$

where \tilde{m}_{shell} , \tilde{m}_{solute} , \tilde{m}_{water} are respectively the complex refractive indices of the shell, solute (assumed to be $1.53 - 10^{-7}i$ ([Wex et al., 2002](#))), and water (i.e. $1.33 - 10^{-7}i$, ([Seinfeld and Pandis, 2006](#))).

The SSA is defined as the ratio of the scattering coefficient to the extinction coefficient of aerosol particles. The scattering and absorption coefficients were calculated from the integration of the corresponding scattering and absorption efficiencies (Q_{sp} and Q_{ap}) over the whole number size distribution:

$$\sigma_{sp/ap} = \int_0^{D_p^{max}} Q_{sp/ap} \cdot \left(\frac{\pi}{4} D_p^2\right) \cdot N(\log D_p) \cdot d \log D_p \quad (10)$$

where Q_{sp} and Q_{ap} can be calculated through the BHCOAT code. Using Eq.(10), the σ_{sp} and σ_{ap} of externally mixed LAC and core-shell mixed aerosol particles can be calculated individually, and then added up to the total σ_{sp} and σ_{ap} . Finally, SSA can be calculated according to its definition.

To calculate the g of aerosol particles, the following equation ([D'Almeida et al., 1991](#)) is used:

$$g = \frac{\sum_i (g_{ext-LAC}^i \sigma_{sp,ext-LAC}^i + g_{core-shell}^i \sigma_{sp,core-shell}^i)}{\sum_i (\sigma_{sp,ext-LAC}^i + \sigma_{sp,core-shell}^i)} \quad (11)$$

where i represents the aerosol size bin, $\sigma_{sp,ext-LAC}^i$ and $\sigma_{sp,core-shell}^i$ is respectively the scattering coefficient of externally mixed LAC and core-shell mixed aerosol particles at corresponding size. $g_{ext-LAC}^i$ and $g_{core-shell}^i$ is respectively the g of externally mixed LAC and core-shell mixed aerosol at each size bin, which can be calculated using the BHCOAT code.

3.2 Calculation of DARE and case design

The calculated aerosol optical properties are used to evaluate the impacts of their diurnal changes on the estimates of daily average DARE. The temporal resolution of SSA and g is about 10 minutes, and hourly average data are used as inputs for radiative transfer model. Some cases are designed to evaluate the impact of diurnal variability of aerosol optical properties on the estimates of daily average DARE.

3.2.1 Calculation of direct aerosol radiative effect

DARE is either evaluated at the TOA or at the surface according to the following equation:

$$F = (f_a \downarrow - f_a \uparrow) - (f_0 \downarrow - f_0 \uparrow) \quad (12)$$

In this expression, F is the DARE, and f denotes the downward/upward irradiance which spans 0.25 μ m to 4 μ m. $(f \downarrow - f \uparrow)$ denotes the net irradiance computed with a given aerosol f_a , or without

216 aerosol f_0 , at either the TOA or surface.

217 The radiative transfer simulations are performed with the Santa Barbara DISORT (discrete
218 ordinates radiative transfer) Atmospheric Radiative Transfer (SBDART) model ([Ricchiazzi et al.,
219 1998](#)). We calculated DARE using the derived SSA and g with diurnal pattern of AOD from an
220 AERONET site, Xianghe. The Angström exponents calculated with the aerosol extinction coefficient
221 at 470 nm and 860 nm are used to account for the spectral dependence of AOD. Moreover, SSA and g
222 at four wavelengths (470 nm, 550 nm, 860 nm and 1240 nm) are used as input of the SBDART model.
223 The atmospheric profile of Mid-Latitude summer provided by SBDART itself is used in simulations.
224 The information of surface albedo is obtained from MCD43C3 albedo product
225 (https://lpdaac.usgs.gov/products/modis_products_table/mcd43c3). And the value of surface albedo at
226 Wuqing at 1 August, 2009 is used to perform the calculation of DARE corresponding to average
227 diurnal variations of AOD, SSA and g , and the surface albedo values for wavelengths at 470 nm, 550
228 nm, 670 nm, 860 nm, 1240 nm, 1640 nm and 2100 nm are 0.152, 0.158, 0.144, 0.212, 0.209, 0.174
229 and 0.119. To obtain the daily average DARE, the calculations are performed with a one-hour time
230 step within the local time range from local time 6:00 to 18:00, and then averaged over 24 hours. The
231 local time range from 6:00 to 18:00 is approximately the time period from sunrise to sunset.

232 3.2.2 Case design

233 Several cases are designed to evaluate the impacts of the diurnal variations of aerosol optical
234 properties on the daily average DARE. The designed cases are listed in Table1. The abbreviation FT
235 stands full temporal. \overline{dt} , \overline{am} and \overline{pm} and \overline{ap} indicate that the aerosol optical properties are
236 averaged over four different time periods: daytime, early morning, late afternoon, and both early
237 morning and late afternoon. Early morning is defined by the period when SZA is within 50° and 70°
238 in the morning, corresponding to local time of 07:00 and 08:00 in this study. Late afternoon is defined
239 by the period when SZA is within 50° and 70° in the afternoon, corresponding to local time of 16:00
240 and 17:00. This specified early morning and late afternoon periods mimic the AERONET sampling
241 periods used for retrieving SSA and g ([Kassianov et al., 2013](#)). Among all these cases, Case 1 is
242 supposed to be the reference case because SSA and g in Case 1 are both for ambient condition with
243 the diurnal changes of AOD also considered. Case 2 is designed to study the impacts of the daily
244 averages of AOD, SSA and g on the DARE. Case 3 to 8 are designed to investigate the sensitivity of

daily average DARE to the diurnal changes of AOD, SSA and g. Case 9 to 11 are designed to test how the daily average DARE responds if the SSA and g are both averaged over either early morning, late afternoon or both early morning and late afternoon. For Case 2 to 11, the actual diurnal variations of selected aerosol optical properties are ignored, and the corresponding averages are used instead.

To estimate the difference between a specified case and the reference case, we define the relative difference (RD) as follow:

$$RD = \frac{F_{case} - F_{case1}}{F_{case1}} \times 100\% \quad (13)$$

where F_{case} is the daily average DARE at TOA/surface of specified case, F_{case1} is the daily average DARE at TOA/surface of Case 1.

4. Results and discussions

4.1 Diurnal variations of aerosol optical properties

The diurnal variation of AOD at 550nm in Xianghe summer is presented in Figure1. AOD at 550nm is calculated using the AOD at 500 nm and the Angström exponent between 440 nm and 675 nm provided by AERONET AOD product. The daily average AOD at 550nm is 0.47, which means that the NCP is highly polluted. The value of AOD between 7 and 8 o'clock in the morning, and that at 16 o'clock in the afternoon are relatively higher, and the relative departures of AOD from daily mean can be up to 20% on average.

Using the method mentioned in Section 3, SSA and g are calculated from the observation. The obtained SSA and g have a temporal resolution of about ten minutes, and are averaged to one-hour data to show their diurnal variations. Those days without a full temporal coverage of SSA or g are excluded, thus, 17 days are available. Only the local time range from 6:00 to 18:00 is considered, since the direct interaction of aerosol with the solar shortwave radiation only happens during daytime.

The average diurnal variations of SSA at 550nm for the ambient and the dry state aerosols during the observation period are illustrated in Figure 2. It can be seen from the graph that the diurnal pattern of SSA at the two states are far different. At dry conditions, the SSA reaches minimum in the morning and evening, and maximum at noon, with an average of 0.86. This result is similar to most previous studies on the diurnal variation of SSA for dry state aerosol(He et al., 2009;Fan et al., 2010;Junwei et

272 [al., 2012; Gyawali et al., 2012](#)). For ambient aerosol, many of the aerosol components are hygroscopic
273 and can take up water as a function of RH ([Bian et al., 2014; Cheng et al., 2008](#)), making the SSA
274 change as the RH changes. In this study, our results demonstrate that the diurnal variation of SSA for
275 ambient aerosol is evident. The SSA reaches maximum in the morning when RH is the highest and
276 minimum in the afternoon, difference between the maximum and minimum can be up to 0.06, with the
277 average at 0.91. Due to the hygroscopic growth of aerosol particles, the scattering coefficient will be
278 largely enhanced when RH is greater than 60% ([Cheng et al., 2008](#)). However, the dependence of
279 aerosol absorption on RH is not as significant as that of scattering ([Redemann et al., 2001; Tao et al.,](#)
280 [2014](#)). According to the definition of SSA, its diurnal variation will be largely influenced by RH,
281 especially when RH is high. The average diurnal pattern of RH during the corresponding period is
282 shown in Figure 3. RH begins to decrease in the morning at 6:00, and reaches minimum in the
283 afternoon. And the RH during this observation period is frequently higher than 60%. Hence, it can be
284 seen from Figure 2 that the diurnal pattern of SSA for ambient aerosol is dominated by but not
285 completely consistent with that of RH. Due to the RH in the afternoon is not high enough, and the SSA
286 of dry state aerosol will play a role. The diurnal pattern of the ratio between the SSA of ambient and
287 dry state aerosol is highly correlated with that of RH, and the daily average ratio is 1.06.

288 The average diurnal patterns of g at 550nm for dry state aerosol and ambient aerosol during the
289 observation period are also illustrated in Figure 2. It is obvious that the diurnal changes of g at two
290 states are quite different. The g of dry state aerosol shows little variability during daytime, and its daily
291 average is 0.62. On the contrary, g of ambient aerosol has evident diurnal variation. Like SSA, the g
292 reaches maximum in the morning when RH is the highest and minimum in the afternoon when RH is
293 the lowest, difference between the maximum and minimum can be up to 0.1, with the average at 0.70.
294 The diurnal pattern of g for ambient aerosol is highly correlated with that of RH. The diurnal pattern
295 of the ratio between g of ambient and dry state aerosol is also consistent with that of RH, and the daily
296 average ratio is 1.12. This can be easily understood, because g of dry state aerosol shows little variation
297 during daytime, the diurnal pattern of g for ambient aerosol is mainly dominated by the diurnal pattern
298 of RH.

299 In addition, the average SSA and g at 440 nm from AERONET site Xianghe during periods from
300 July to August of years from 2001 to 2013 are also shown in Figure 2 (a) and (d), respectively. There

are 91 days available for SSA with both morning and afternoon observation valid, and 144 days for g . The results demonstrate that the evident morning to afternoon contrast of SSA and g mentioned before are not seen in SSA and g observed from AERONET measurements. In those AERONET results, g in the early morning is slightly higher than that in the late afternoon, however, on the contrary, SSA in the late afternoon is slightly higher than that in the early morning. Two reasons may be responsible for this discrepancy: (1) the SSA and g calculated in this research is based on in-situ measurements, however, SSA and g provided by AERONET measurements are columnar properties; (2) different time periods of those two datasets.

4.2 The impacts of diurnal variations of aerosol optical properties on the estimation of daily average DARE

The average diurnal pattern of AOD, SSA and g introduced in Section 4.1 are used to estimate the overall influence of their diurnal changes on the estimation of DARE. The influences at TOA and surface are evaluated separately, and the designed cases are introduced in Section 3.2.2. Results of this assessment are shown in Figure 4, corresponding to TOA and surface respectively. The 24h average DARE for Case 1 at TOA and Surface are -8.28 and -32.51 W/m^2 , respectively. The small differences in Case 2 at TOA and surface demonstrate that an accurate prediction of daily average DARE can be achieved by using the daily averages of AOD, SSA and g , even when their diurnal variations are all evident. For Case 3, it leads to an overestimation of the negative daily average DARE at TOA and surface, due to the overestimation of AOD averaged over early morning. This means, if the temporal coverage of AOD is incomplete, it might result in a large bias in the estimation of daily average DARE at TOA and surface when the diurnal variation of AOD is significant. A similar conclusion is reached from previous studies([Arola et al., 2013](#); [Kassianov et al., 2013](#)). However, for Case 4, due to the AOD averaged over late afternoon is very close to its daytime average, the relative difference is very small. In Case 5 and 6, the SSA averaged over the early morning or late afternoon is used. As a result, the estimated daily average DARE shows large biases. A larger SSA will cause less absorbing of incident solar radiation by atmospheric aerosol, more light reaches the surface and reflected into space. The overestimation of SSA in the early morning will therefore result in a stronger negative radiative effect (NRE) at TOA and weaker NRE at surface. In Case 7 and 8, the g averaged over the early morning or late afternoon is used, it will also lead to large biases in the estimation of daily average DARE at TOA.

330 With the increase of g , more light will be forward scattered, absorbed by the atmospheric aerosol, and
331 reaches the surface. Consequently, the overestimation of g in the early morning will result in weaker
332 NRE at TOA and surface. The results from Case 5 to 8 indicate the diurnal variations of SSA and g in
333 the NCP have significant impacts on the estimation of DARE at TOA, but less impacts on the
334 estimation of DARE at surface. If the temporal resolution of SSA and g is not high enough to accurately
335 represent their diurnal variations, the estimated daily average DARE at TOA might be biased
336 significantly.

337 In Case 9, the SSA and g are both averaged over early morning, and daily average AOD is used.
338 The results show that this treatment has less influence on the estimation of daily average DARE at
339 TOA, but larger influences at surface than those in Case 5 and 7. According to the analysis of Case 5
340 to 8, the overestimation of SSA will lead to stronger NRE at TOA and weaker NRE at surface. The
341 overestimation of g will result in weaker NRE at TOA and surface. The effect of the overestimation of
342 SSA and g will be cancelled out to some extent at TOA, but enhanced at the surface, and vice versa in
343 Case 10. In Case 11, the results demonstrate that both SSA and g averaged over early morning and late
344 afternoon only has little influence on the estimation of daily average DARE at TOA and surface.
345 Conclusions can be made that, overall, for estimating DARE at TOA, schemes of Case 9 to 11 can
346 largely improve the results compared to Case 5 to 8. Case 11 is the best and also suitable for estimating
347 DARE at surface.

348 The RD results of cases at TOA for individual days with specific diurnal variations of SSA and g ,
349 and also the absolute values and day-to-day variability of DARE for Case 1 are shown in Figure 5.
350 The diurnal patterns of AOD for all days are fixed, and is the same as the one introduced in Section
351 4.1. This means that the evident day-to-day variability of DARE for Case 1 shown in Figure 5 is driven
352 by the day-to-day variability of SSA and g . Overall, the RD results from cases shown in Figure 5c for
353 different days are consistent with the results from cases aforementioned. For Case 2, its results are very
354 stable and close to zero which means that even the diurnal patterns of SSA and g are not completely
355 consistent with the their average pattern introduced in Section 4.1, their daytime averages are enough
356 to provide a accurate estimation of DARE. For Case 3 and 4, due to the diurnal patterns of AOD for
357 17 valid days are the same one, their results vary little among 17 selected days. For Case 5 to 8, it can
358 be seen from Figure 5, high variability existed in their results. Using Case 5 as an example, it

corresponds to the case in which the daytime average of AOD and g , and the early morning average of SSA are used. Hence its variation compare to Case 2 is induced by the variation of the difference between the early morning average and daytime average of SSA (DEDSSA). The day-to-day variation of DEDSSA is presented in Figure 6, it is clear that its variability is consistent with the variability of RD results of Case 5 shown in Figure 5c. In addition, the differences between the early morning average and day time average of RH (DEDRH) are also shown in Figure 6, it shows that the pattern of day-to-day variation of DEDSSA is completely consistent with the pattern of DEDRH. This results demonstrate that the high variability of the RD results of Case 5 is driven by the variation of RH, and also the results of Case 6 to 8. For Case 9 to 11, their performances are much better than those of Case 5 to 8. In particular, the results of Case 11 are very stable and close to the results of Case 2. This means that, even if the diurnal variations of SSA and g are not in exact accordance with the average pattern mentioned in Section 4.1, the scheme of Case 11 still can lead to a good result. But exception still exists for Case 11, the relative difference in Julian day of 197 is notably larger than that in other days, and the least improvement compare to results of other cases. It is found that the diurnal variation of RH at this day is far different from the one introduced in Section 4.1. The diurnal variations of SSA, g and RH at Julian day of 197 are shown in Figure 7. It's clear that the diurnal variations of SSA and g are dominated by the diurnal variation of RH, but not like their typical pattern in those selected days. There are two reasons that the results of Case 11 are very small and stable in most of days. First, the diurnal pattern of SSA and g are both dominated by the diurnal variation of RH, thus the SSA and g are both highest in the dawn and lowest in the late afternoon, the SSA and g averaged over early morning and late afternoon will be closer to their daily averages than Case 9 and 10. Second, according to the analysis for the results of Case 9 and 10, the SSA and g have opposite effects on the estimation of daily averaged DARE at TOA, the influence of SSA will be offset to some extent by that of g . Therefore, the diurnal pattern of RH is an important factor which determines if the scheme of Case 11 can be used to improve the estimation of daily average DARE. On the other hand, the results of Case 9 and 10 are not as stable as that of Case 11, but still much better than those of Case 5 to 8. The diurnal pattern of RH shown in Figure 3 is prevalent in many regions around the world([Ephrath et al., 1996](#);[Gebhart et al., 2001](#);[Fan et al., 2010](#);[Sun et al., 2013](#)), the scheme of Case 11 maybe also suitable for these regions when the RH is frequently higher than 60%, especially for regions where aerosol particles are similarly or more hygroscopic compared to the hygroscopicity of aerosols introduced in

this research. We suggest that using the scheme of Case 11 to improve the accurate estimation of DARE. If the temporal samplings of SSA and g are too few to adopt the scheme of Case 11, schemes of Case 9 and 10 still can be good options for improving the estimation of DARE at TOA. The results of Case 5 to 8 demonstrate that the diurnal changes of SSA and g have significant influences on the estimation of DARE. However, the RD results of Case 11 are much smaller than the day-to-day variability of DARE for Case 1 shown in Figure 5b, which indicate that if the diurnal patterns of SSA and g are consistent with those introduced in this research, observing incomplete diurnal cycles of SSA and g have only second-order consequences on direct radiative effect estimates.

5. Conclusions

SSA and g are both important parameters in the estimation of DARE ([McComiskey et al., 2008](#)), but their diurnal variations are rarely investigated, especially in the NCP. In this paper, using the in-situ measurements from HaChi campaign, the diurnal variations of SSA and g are studied. The results show that, for ambient aerosol, the diurnal patterns of SSA and g are both highest in the dawn and lowest in the late afternoon, and far different from those of dry state aerosol. For dry state aerosol, the SSA reaches minimum in the morning and evening, and maximum at noon, with the average at 0.86. For ambient aerosol, the SSA reaches maximum in the dawn when RH is the highest and minimum in the afternoon, difference between the maximum and minimum can be up to 0.06, with the average at 0.91. The diurnal pattern of SSA for ambient aerosol is dominated by that of RH, and the average ratio between the SSA of ambient and dry state aerosol is 1.06. On the other hand, the g of dry state aerosol shows little variability during daytime, with an average of 0.62. The diurnal pattern of g for ambient aerosol is also evident and dominated by that of RH, the difference between the maximum and minimum can be up to 0.1, with an average of 0.70. The average ratio of g for ambient aerosol to that for dry state aerosol is 1.12.

Using the SSA and g calculated from in-situ measurements, and AOD from AERONET measurements, several cases are designed to evaluate the impacts of the diurnal changes of AOD, SSA and g on the estimates of daily average DARE. The results demonstrate that the diurnal changes of SSA and g in the NCP have significant influence on the estimation of DARE at TOA, which means that if the temporal samplings of SSA and g are incomplete, significant errors may occur in the estimation of DARE at TOA. If the full temporal coverage of AOD, SSA and g are available, the

accurate estimation of DARE can be achieved by using the daily averages of AOD, SSA and g. However, due to the lack of full temporal coverage datasets of SSA and g, their daily averages are usually not available. Regarding this, three cases are designed in order to find some suggestions about the estimation of daily average DARE. We conclude that, if the RH plays a dominant role in the diurnal variations of SSA and g, an accurate estimation of DARE can be achieved by using SSA and g averaged over early morning and late afternoon as inputs for radiative transfer model. If the samplings of SSA or g are only available in the early morning or late afternoon, either averaged over early morning or late afternoon of both SSA and g can be used to improve the estimation of DARE at TOA. Those important findings indicate that the diurnal changes of SSA and g have significant influence on the estimation of DARE. However, if the diurnal patterns of SSA and g are consistent with those introduced in this research, observing incomplete diurnal cycles of SSA and g have only second-order consequences on direct radiative effect estimates. It may allow one to bypass the complex temporal monitoring problems associated with significant diurnal changes of SSA and g. This study will further our understanding of the diurnal characteristics of SSA and g in the NCP and help for improving the accurate estimation of DARE.

Acknowledgment

We acknowledge the free use of MODIS surface albedo product and AOD measurements from AERONET. This work is supported by the National 973 project of China (2011CB403402), the National Natural Science Foundation of China (41375134) and the Beijing Natural Science Foundation (8131003).

References

- Arola, A., Eck, T. F., Huttunen, J., Lehtinen, K. E. J., Lindfors, A. V., Myhre, G., Smirnov, A., Tripathi, S. N., and Yu, H.: Influence of observed diurnal cycles of aerosol optical depth on aerosol direct radiative effect, *Atmospheric Chemistry and Physics*, 13, 7895-7901, 10.5194/acp-13-7895-2013, 2013.
- Bellouin, N., Boucher, O., Haywood, J., and Reddy, M. S.: Global estimate of aerosol direct radiative forcing from satellite measurements, *Nature*, 438, 1138-1141, 10.1038/nature04348, 2005.
- Bellouin, N., Jones, A., Haywood, J., and Christopher, S. A.: Updated estimate of aerosol direct radiative forcing from satellite observations and comparison against the Hadley Centre climate model, *Journal of Geophysical Research: Atmospheres*, 113, D10205, 10.1029/2007JD009385, 2008.
- Bellouin, N., Quaas, J., Morcrette, J.-J., and Boucher, O.: Estimates of aerosol radiative forcing from the MACC re-analysis, *Atmospheric Chemistry and Physics*, 13, 2045-2062, 2013.

451 Bian, Y. X., Zhao, C. S., Ma, N., Chen, J., and Xu, W. Y.: A study of aerosol liquid water content based on hygroscopicity
 452 measurements at high relative humidity in the North China Plain, *Atmos. Chem. Phys.*, 14, 6417-6426, 10.5194/acp-14-
 453 6417-2014, 2014.

454 Birmili, W., Stratmann, F., and Wiedensohler, A.: Design of a DMA-based size spectrometer for a large particle size range
 455 and stable operation, *Journal of Aerosol Science*, 30, 549-553, 10.1016/S0021-8502(98)00047-0, 1999.

456 Bohren, C. F., and Huffman, D. R.: *Absorption and scattering of light by small particles*, Wiley, New York, USA, 2008.

457 Bond, T. C., Doherty, S. J., Fahey, D., Forster, P., Berntsen, T., DeAngelo, B., Flanner, M., Ghan, S., Kärcher, B., and Koch, D.:
 458 Bounding the role of black carbon in the climate system: A scientific assessment, *Journal of Geophysical Research:*
 459 *Atmospheres*, 118, 5380-5552, 2013.

460 Boucher, O.: On aerosol direct shortwave forcing and the Henyey-Greenstein phase function, *Journal of the Atmospheric*
 461 *Sciences*, 55, 128-134, 10.1175/1520-0469(1998)055<0128:oadsfa>2.0.co;2, 1998.

462 Chen, J., Zhao, C. S., Ma, N., Liu, P. F., Göbel, T., Hallbauer, E., Deng, Z. Z., Ran, L., Xu, W. Y., Liang, Z., Liu, H. J., Yan, P., Zhou,
 463 X. J., and Wiedensohler, A.: A parameterization of low visibilities for hazy days in the North China Plain, *Atmos. Chem.*
 464 *Phys.*, 12, 4935-4950, 10.5194/acp-12-4935-2012, 2012.

465 Cheng, Y., Wiedensohler, A., Eichler, H., Heintzenberg, J., Tesche, M., Ansmann, A., Wendisch, M., Su, H., Althausen, D.,
 466 and Herrmann, H.: Relative humidity dependence of aerosol optical properties and direct radiative forcing in the surface
 467 boundary layer at Xinken in Pearl River Delta of China: An observation based numerical study, *Atmospheric Environment*,
 468 42, 6373-6397, 2008.

469 Cheng, Y. F., Berghof, M., Garland, R. M., Wiedensohler, A., Wehner, B., Müller, T., Su, H., Zhang, Y. H., Achtert, P., Nowak,
 470 A., Pöschl, U., Zhu, T., Hu, M., and Zeng, L. M.: Influence of soot mixing state on aerosol light absorption and single
 471 scattering albedo during air mass aging at a polluted regional site in northeastern China, *Journal of Geophysical Research:*
 472 *Atmospheres*, 114, D00G10, 10.1029/2008JD010883, 2009.

473 Chung, C. E., Ramanathan, V., Kim, D., and Podgorny, I. A.: Global anthropogenic aerosol direct forcing derived from
 474 satellite and ground-based observations, *Journal of Geophysical Research-Atmospheres*, 110, 17, 10.1029/2005jd006356,
 475 2005.

476 D'Almeida, G. A., Koepke, P., and Shettle, E. P.: *Atmospheric aerosols: global climatology and radiative characteristics*, A.
 477 Deepak Pub., 1991.

478 Dubovik, O., Smirnov, A., Holben, B., King, M., Kaufman, Y., Eck, T., and Slutsker, I.: Accuracy assessments of aerosol optical
 479 properties retrieved from Aerosol Robotic Network (AERONET) Sun and sky radiance measurements, *Journal of*
 480 *Geophysical Research: Atmospheres* (1984–2012), 105, 9791-9806, 2000.

481 Ephraïm, J. E., Goudriaan, J., and Marani, A.: Modelling diurnal patterns of air temperature, radiation wind speed and
 482 relative humidity by equations from daily characteristics, *Agricultural Systems*, 51, 377-393,
 483 [http://dx.doi.org/10.1016/0308-521X\(95\)00068-G](http://dx.doi.org/10.1016/0308-521X(95)00068-G), 1996.

484 Fan, X., Chen, H., Xia, X., Li, Z., and Cribb, M.: Aerosol optical properties from the Atmospheric Radiation Measurement
 485 Mobile Facility at Shouxian, China, *Journal of Geophysical Research-Atmospheres*, 115, 10.1029/2010jd014650, 2010.

486 Gebhart, K. A., Copeland, S., and Malm, W. C.: Diurnal and seasonal patterns in light scattering, extinction, and relative
 487 humidity, *Atmospheric Environment*, 35, 5177-5191, [http://dx.doi.org/10.1016/S1352-2310\(01\)00319-3](http://dx.doi.org/10.1016/S1352-2310(01)00319-3), 2001.

488 Gyawali, M., Arnott, W. P., Zaveri, R. A., Song, C., Moosmüller, H., Liu, L., Mishchenko, M. I., Chen, L. W. A., Green, M. C.,
 489 Watson, J. G., and Chow, J. C.: Photoacoustic optical properties at UV, VIS, and near IR wavelengths for laboratory
 490 generated and winter time ambient urban aerosols, *Atmospheric Chemistry and Physics*, 12, 2587-2601, 10.5194/acp-12-
 491 2587-2012, 2012.

492 He, X., Li, C. C., Lau, A. K. H., Deng, Z. Z., Mao, J. T., Wang, M. H., and Liu, X. Y.: An intensive study of aerosol optical
 493 properties in Beijing urban area, *Atmospheric Chemistry and Physics*, 9, 8903-8915, 2009.

494 Hennig, T., Massling, A., Brechtel, F. J., and Wiedensohler, A.: A tandem DMA for highly temperature-stabilized hygroscopic

495 particle growth measurements between 90% and 98% relative humidity, *Journal of Aerosol Science*, 36, 1210-1223,
 496 10.1016/j.jaerosci.2005.01.005, 2005.

497 Holben, B., Eck, T., Slutsker, I., Tanre, D., Buis, J., Setzer, A., Vermote, E., Reagan, J., Kaufman, Y., and Nakajima, T.:
 498 AERONET—A federated instrument network and data archive for aerosol characterization, *Remote sensing of*
 499 *environment*, 66, 1-16, 1998.

500 Holben, B., Eck, T., Slutsker, I., Smirnov, A., Sinyuk, A., Schafer, J., Giles, D., and Dubovik, O.: AERONET's version 2.0 quality
 501 assurance criteria, *Asia-Pacific Remote Sensing Symposium*, 2006, 64080Q-64080Q-64014,

502 Junwei, X., Jun, T., Renjian, Z., Tiantao, C., Chunpeng, L., Jianmin, C., Guanghan, H., Xiang, L., and Zhaoqin, Z.:
 503 Measurements of surface aerosol optical properties in winter of Shanghai, *Atmospheric Research*, 109-110, 25-35,
 504 10.1016/j.atmosres.2012.02.008, 2012.

505 Kassianov, E., Barnard, J., Pekour, M., Berg, L. K., Michalsky, J., Lantz, K., and Hodges, G.: Do diurnal aerosol changes affect
 506 daily average radiative forcing?, *Geophys. Res. Lett.*, 2013.

507 Kaufman, Y. J., Holben, B. N., Tanré, D., Slutsker, I., Smirnov, A., and Eck, T. F.: Will aerosol measurements from Terra and
 508 Aqua Polar Orbiting satellites represent the daily aerosol abundance and properties?, *Geophys. Res. Lett.*, 27, 3861-3864,
 509 10.1029/2000GL011968, 2000.

510 Liu, H. J., Zhao, C. S., Nekat, B., Ma, N., Wiedensohler, A., van Pinxteren, D., Spindler, G., Müller, K., and Herrmann, H.:
 511 Aerosol hygroscopicity derived from size-segregated chemical composition and its parameterization in the North China
 512 Plain, *Atmos. Chem. Phys.*, 14, 2525-2539, 10.5194/acp-14-2525-2014, 2014.

513 Liu, P. F., Zhao, C. S., Göbel, T., Hallbauer, E., Nowak, A., Ran, L., Xu, W. Y., Deng, Z. Z., Ma, N., Mildemberger, K., Henning,
 514 S., Stratmann, F., and Wiedensohler, A.: Hygroscopic properties of aerosol particles at high relative humidity and their
 515 diurnal variations in the North China Plain, *Atmos. Chem. Phys.*, 11, 3479-3494, 10.5194/acp-11-3479-2011, 2011.

516 Ma, N., Zhao, C. S., Nowak, A., Müller, T., Pfeifer, S., Cheng, Y. F., Deng, Z. Z., Liu, P. F., Xu, W. Y., Ran, L., Yan, P., Göbel, T.,
 517 Hallbauer, E., Mildemberger, K., Henning, S., Yu, J., Chen, L. L., Zhou, X. J., Stratmann, F., and Wiedensohler, A.: Aerosol
 518 optical properties in the North China Plain during HaChi campaign: an in-situ optical closure study, *Atmos. Chem. Phys.*,
 519 11, 5959-5973, 10.5194/acp-11-5959-2011, 2011.

520 Ma, N., Zhao, C. S., Müller, T., Cheng, Y. F., Liu, P. F., Deng, Z. Z., Xu, W. Y., Ran, L., Nekat, B., van Pinxteren, D., Gnauk, T.,
 521 Müller, K., Herrmann, H., Yan, P., Zhou, X. J., and Wiedensohler, A.: A new method to determine the mixing state of light
 522 absorbing carbonaceous using the measured aerosol optical properties and number size distributions, *Atmos. Chem. Phys.*,
 523 12, 2381-2397, 10.5194/acp-12-2381-2012, 2012.

524 Mazzola, M., Lanconelli, C., Lupi, A., Busetto, M., Vitale, V., and Tomasi, C.: Columnar aerosol optical properties in the Po
 525 Valley, Italy, from MFRSR data, *Journal of Geophysical Research-Atmospheres*, 115, 17, 10.1029/2009jd013310, 2010.

526 McComiskey, A., Schwartz, S. E., Schmid, B., Guan, H., Lewis, E. R., Ricchiazzi, P., and Ogren, J. A.: Direct aerosol forcing:
 527 Calculation from observables and sensitivities to inputs, *Journal of Geophysical Research: Atmospheres* (1984–2012), 113,
 528 2008.

529 Myhre, G.: Consistency between satellite-derived and modeled estimates of the direct aerosol effect, *Science*, 325, 187-
 530 190, 2009.

531 Myhre, G., Samset, B., Schulz, M., Balkanski, Y., Bauer, S., Berntsen, T., Bian, H., Bellouin, N., Chin, M., and Diehl, T.:
 532 Radiative forcing of the direct aerosol effect from AeroCom Phase II simulations, *Atmospheric Chemistry & Physics*, 13,
 533 2013.

534 Petters, M. D., and Kreidenweis, S. M.: A single parameter representation of hygroscopic growth and cloud condensation
 535 nucleus activity, *Atmospheric Chemistry and Physics*, 7, 1961-1971, 2007.

536 Ran, L., Zhao, C. S., Xu, W. Y., Lu, X. Q., Han, M., Lin, W. L., Yan, P., Xu, X. B., Deng, Z. Z., Ma, N., Liu, P. F., Yu, J., Liang, W. D.,
 537 and Chen, L. L.: VOC reactivity and its effect on ozone production during the HaChi summer campaign, *Atmos. Chem.*
 538 *Phys.*, 11, 4657-4667, 10.5194/acp-11-4657-2011, 2011.

Redemann, J., Russell, P. B., and Hamill, P.: Dependence of aerosol light absorption and single-scattering albedo on ambient relative humidity for sulfate aerosols with black carbon cores, *Journal of Geophysical Research-Atmospheres*, 106, 27485-27495, 10.1029/2001jd900231, 2001.

Remer, L. A., and Kaufman, Y. J.: Aerosol direct radiative effect at the top of the atmosphere over cloud free ocean derived from four years of MODIS data, *Atmospheric Chemistry and Physics*, 6, 237-253, 2006.

Ricchiazzi, P., Yang, S., Gautier, C., and Sowle, D.: SBDART: A research and teaching software tool for plane-parallel radiative transfer in the Earth's atmosphere, *Bull. Amer. Meteorol. Soc.*, 79, 2101-2114, 1998.

Seinfeld, J. H., and Pandis, S. N.: *Atmospheric chemistry and physics: from air pollution to climate change*, John Wiley & Sons, 2006.

Sena, E., Artaxo, P., and Correia, A.: Spatial variability of the direct radiative forcing of biomass burning aerosols and the effects of land use change in Amazonia, *Atmospheric Chemistry and Physics*, 13, 1261-1275, 2013.

Smirnov, A., Holben, B. N., Eck, T. F., Slutsker, I., Chatenet, B., and Pinker, R. T.: Diurnal variability of aerosol optical depth observed at AERONET (Aerosol Robotic Network) sites, *Geophys. Res. Lett.*, 29, 4, 10.1029/2002gl016305, 2002.

Su, W., Loeb, N. G., Schuster, G. L., Chin, M., and Rose, F. G.: Global all - sky shortwave direct radiative forcing of anthropogenic aerosols from combined satellite observations and GOCART simulations, *Journal of Geophysical Research: Atmospheres*, 118, 655-669, 2013.

Sun, Y., Zhou, X., Wai, K., Yuan, Q., Xu, Z., Zhou, S., Qi, Q., and Wang, W.: Simultaneous measurement of particulate and gaseous pollutants in an urban city in North China Plain during the heating period: Implication of source contribution, *Atmospheric Research*, 134, 24-34, <http://dx.doi.org/10.1016/j.atmosres.2013.07.011>, 2013.

Tao, J. C., Zhao, C. S., Ma, N., and Liu, P. F.: The impact of aerosol hygroscopic growth on the single-scattering albedo and its application on the NO₂ photolysis rate coefficient, *Atmos. Chem. Phys.*, 14, 12055-12067, 10.5194/acp-14-12055-2014, 2014.

Wex, H., Neususs, C., Wendisch, M., Stratmann, F., Koziar, C., Keil, A., Wiedensohler, A., and Ebert, M.: Particle scattering, backscattering, and absorption coefficients: An in situ closure and sensitivity study, *Journal of Geophysical Research-Atmospheres*, 107, 18, 10.1029/2000jd000234, 2002.

Xu, W. Y., Zhao, C. S., Ran, L., Deng, Z. Z., Liu, P. F., Ma, N., Lin, W. L., Xu, X. B., Yan, P., He, X., Yu, J., Liang, W. D., and Chen, L. L.: Characteristics of pollutants and their correlation to meteorological conditions at a suburban site in the North China Plain, *Atmos. Chem. Phys.*, 11, 4353-4369, 10.5194/acp-11-4353-2011, 2011.

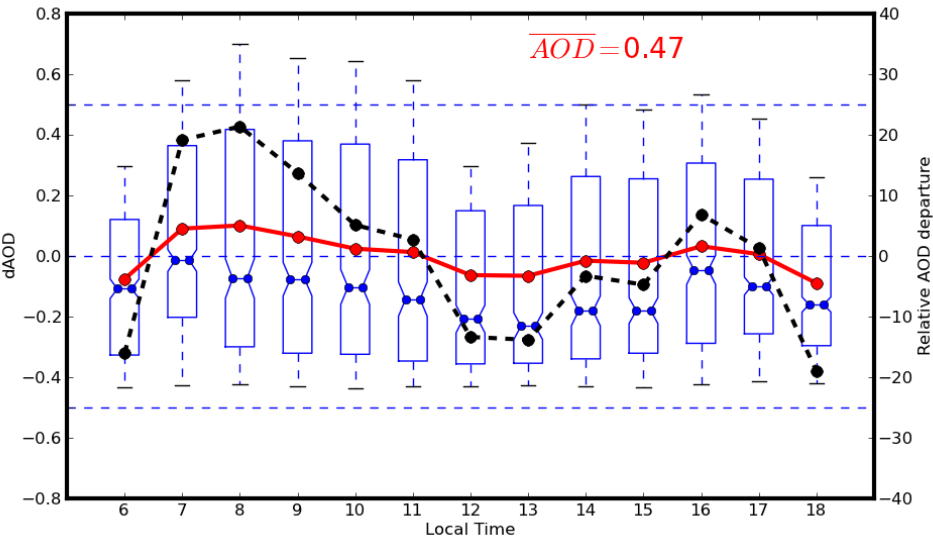
Zhang, Y., Yu, H., Eck, T. F., Smirnov, A., Chin, M., Remer, L. A., Bian, H., Tan, Q., Levy, R., and Holben, B. N.: Aerosol daytime variations over North and South America derived from multiyear AERONET measurements, *Journal of Geophysical Research: Atmospheres* (1984–2012), 117, 2012.

Zhao, C., Tie, X., and Lin, Y.: A possible positive feedback of reduction of precipitation and increase in aerosols over eastern central China, *Geophys. Res. Lett.*, 33, L11814, 10.1029/2006GL025959, 2006.

583 **Table 1.** designed cases

	case1	case2	case3	case4	case5	case6	case7	case8	case9	case10	case11
AOD	FT	\overline{dt}	\overline{am}	\overline{pm}	\overline{dt}	\overline{dt}	\overline{dt}	\overline{dt}	\overline{dt}	\overline{dt}	\overline{dt}
SSA	FT	\overline{dt}	\overline{dt}	\overline{dt}	\overline{am}	\overline{pm}	\overline{dt}	\overline{dt}	\overline{am}	\overline{pm}	\overline{ap}
g	FT	\overline{dt}	\overline{dt}	\overline{dt}	\overline{dt}	\overline{dt}	\overline{am}	\overline{pm}	\overline{am}	\overline{pm}	\overline{ap}

FT : full temporal; \overline{dt} : averaged over daytime(6:00 to 18:00), \overline{am} : averaged over early morning; \overline{pm} : averaged over late afternoon; \overline{ap} : averaged over early morning and late afternoon; early morning: $50^\circ \leq SZA \leq 70^\circ$ in the morning; late afternoon: $50^\circ \leq SZA \leq 70^\circ$ in the afternoon.



590
591 **Figure 1.** The average diurnal pattern of AOD at 550 nm from AERONET measurements, Xianghe summer. Red line
592 represents the absolute AOD departures (dAOD) from daily mean. Box plots give absolute AOD departure range from
593 25th to 75th percentile, and bars outside the boxes give the range within 5th to 95th percentile, the blue dots in the box are
594 medians. Black solid points give the relative departures in the right axis.

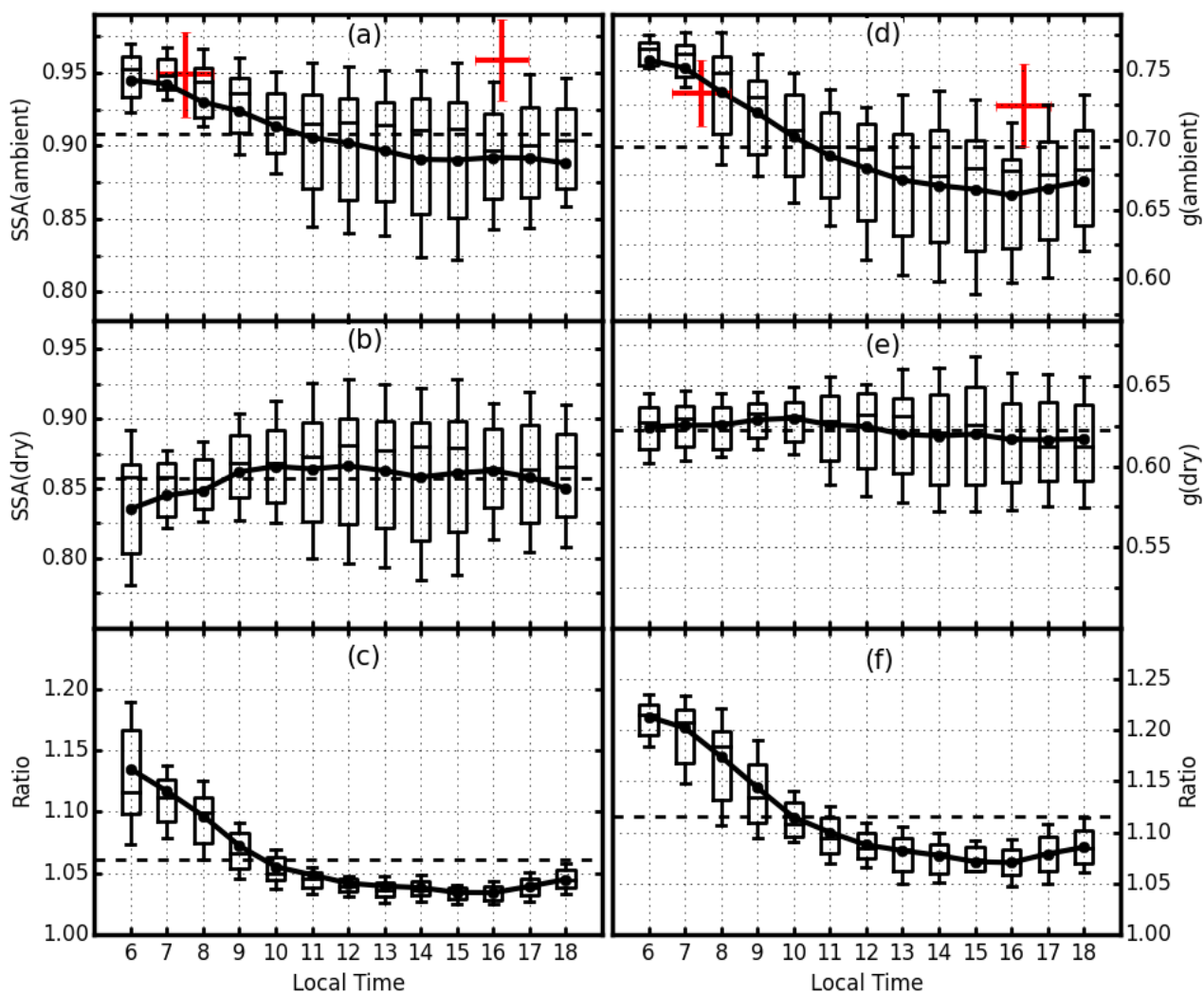
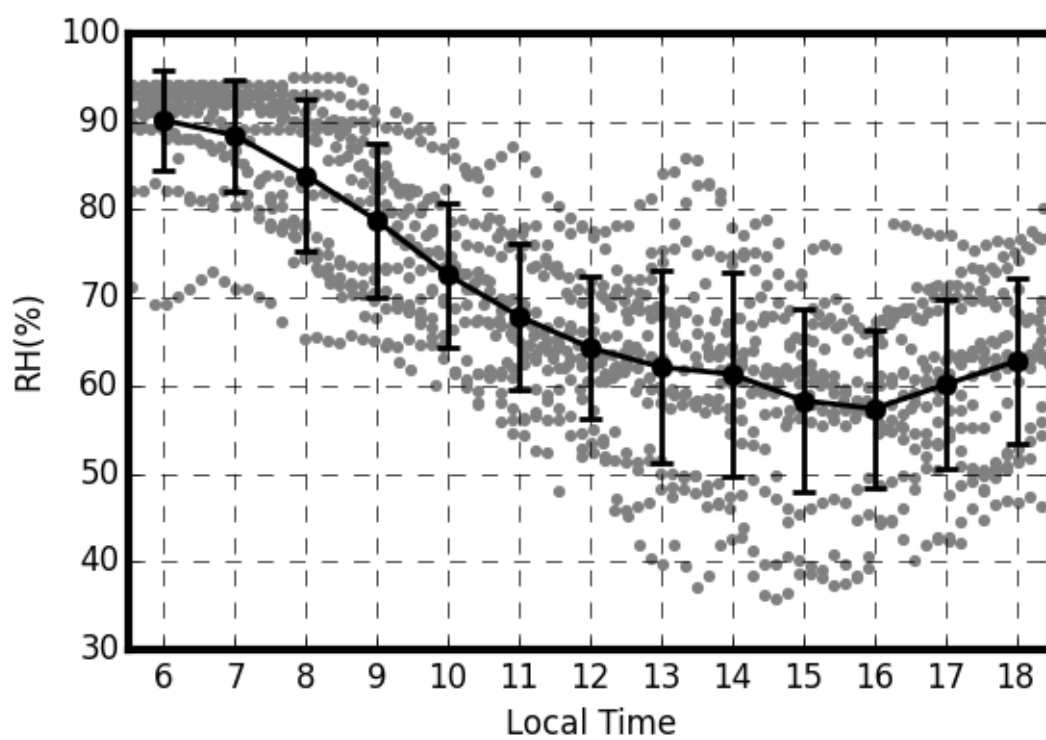


Figure 2. The diurnal variations of SSA and g at 550 nm, (a) average diurnal pattern of SSA for ambient aerosol and average SSA at 440 nm from AERONET site Xianghe (red plus symbol) ; (b) average diurnal pattern of SSA for dry state aerosol; (c) the ratio between (a) and (b); (d) average diurnal pattern of g for ambient aerosol and average g at 440 nm from AERONET site Xianghe (red plus symbol); (e) average diurnal pattern of g for dry state aerosol; (f) The ratio between (d) and (e). Black lines are the average diurnal variations, and dashed lines are their corresponding averages. Box plots give the data points range from 25th to 75th percentile, and bars outside the boxes give the range within 5th to 95th percentile. Lines in boxes are medians. The x and y dimensions of the red plus symbol represent the standard deviations of SSA or g and the local time when data points are sampled, respectively.

617
618
619
620
621
622



623
624
625
626
627
628
629
630
631

Figure 3. The scatter plots of RH for selected days, the black line is the average diurnal variation of RH.

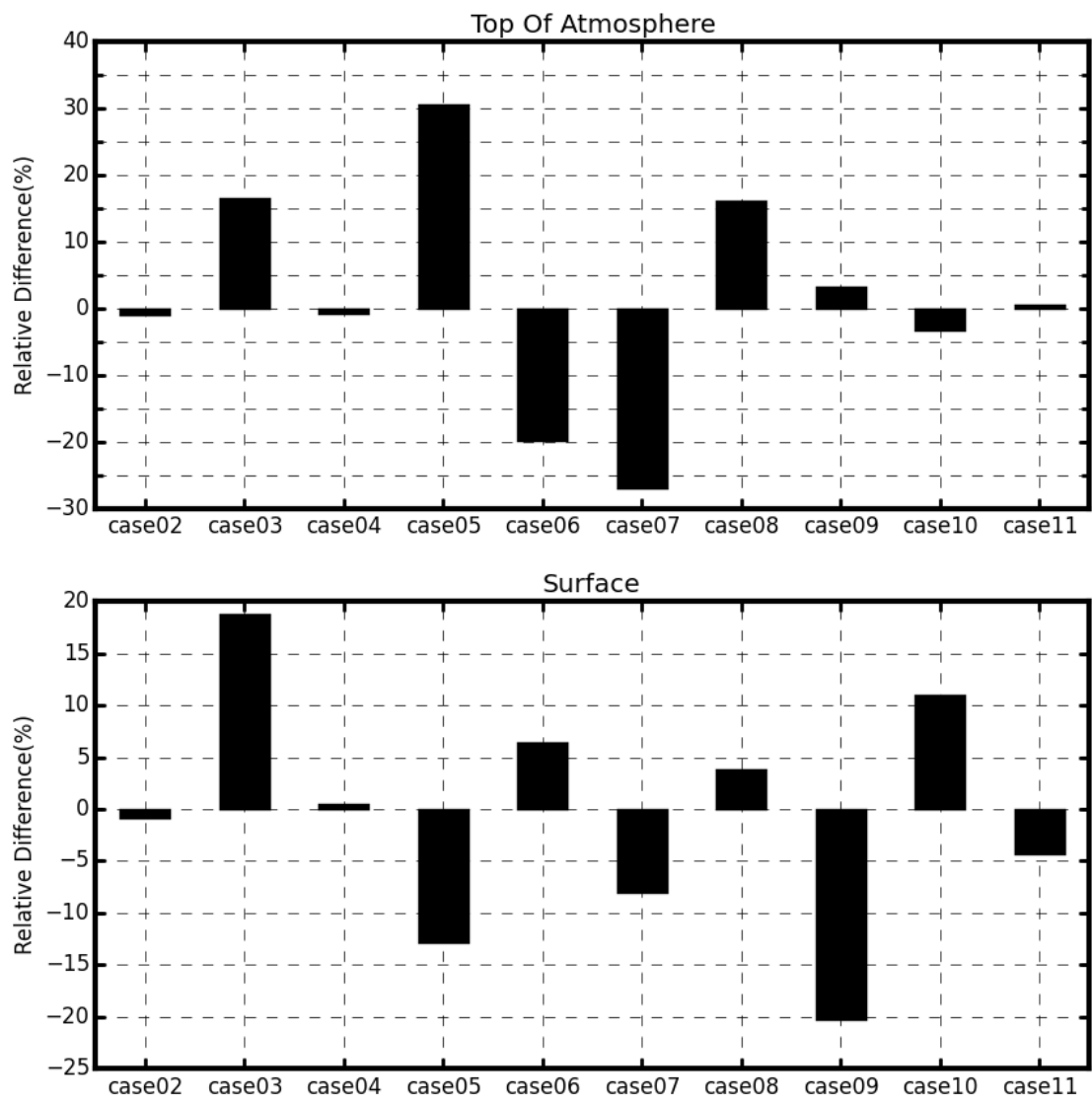


Figure 4. Relative Differences compared to Case 1 of different cases at TOA and surface.

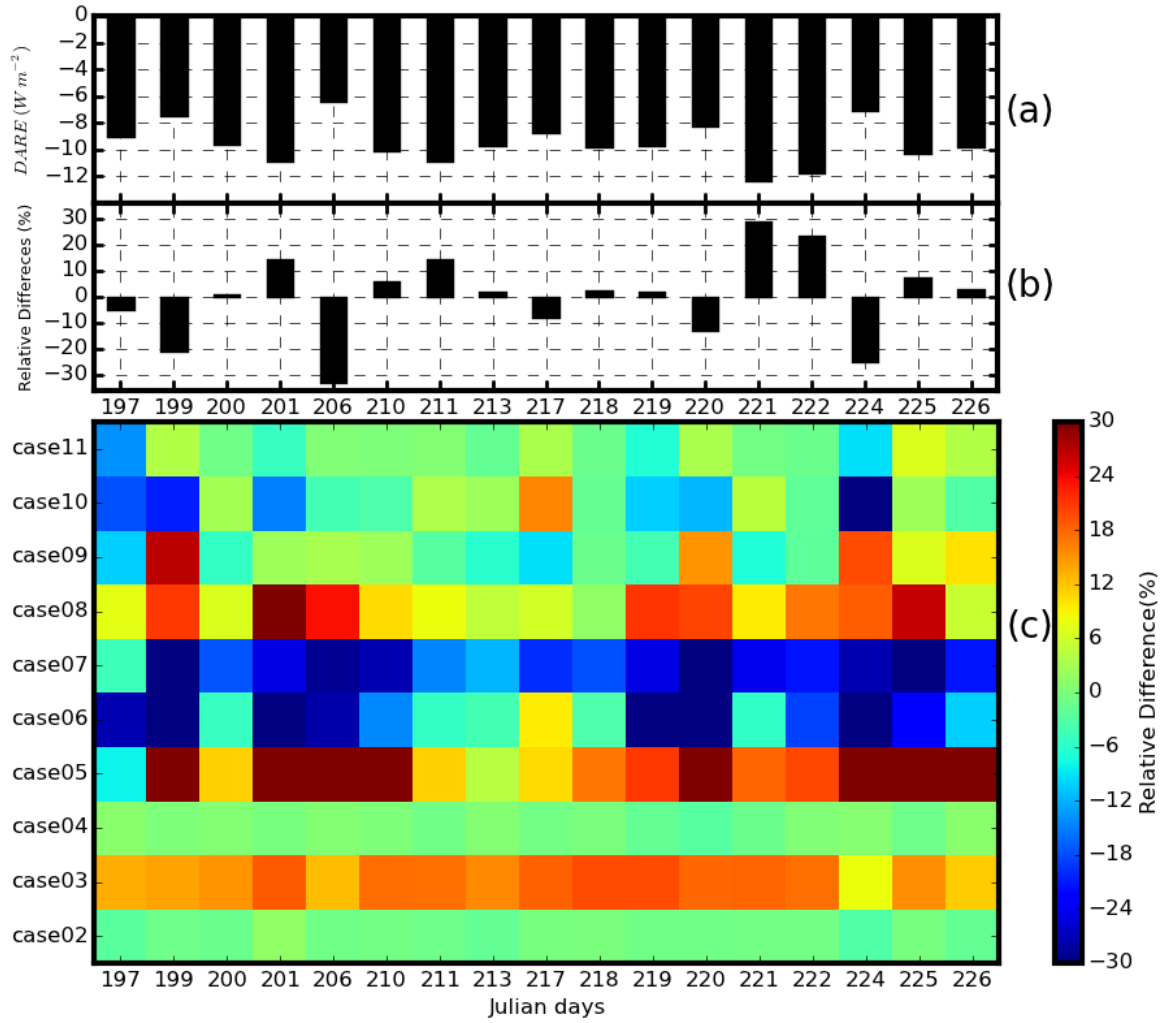
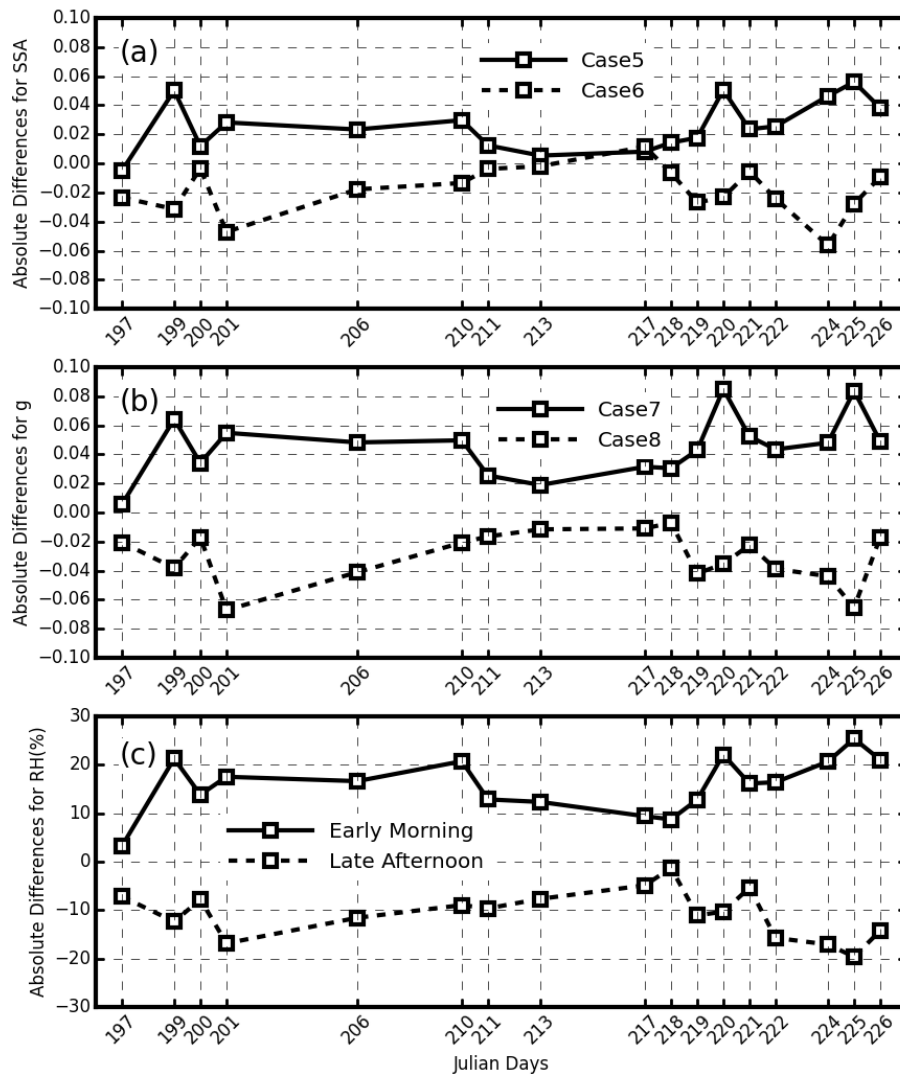


Figure 5. (a) The absolute values of 24h average DARE in W/m^2 at TOA for Case 1; (b):The relative differences of DARE values at TOA of Case 1 compared to its 17-day average; (c): The Relative Differences compared to Case 1 of different cases for different days at TOA



646

647 **Figure 6.** The absolute differences between early morning (or late afternoon) average and the daytime average of SSA, g,

648 and RH. (a) For SSA: corresponding to Case 5 and 6; (b) For g: corresponding to Case 7 and 8; (c) For RH.

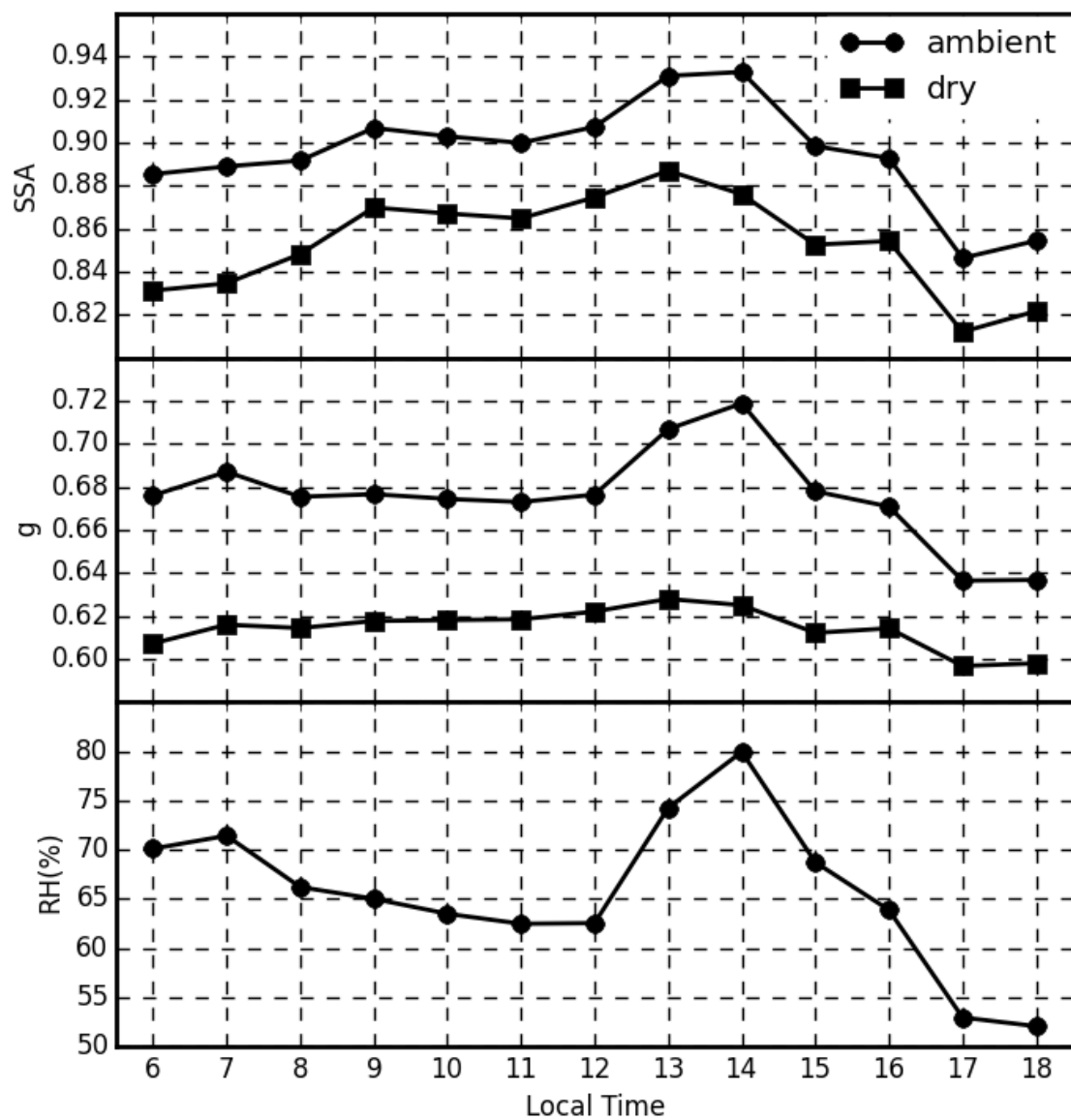


Figure 7. The diurnal variations of SSA, g and RH at the Julian day of 197